J. Fluid Mech. (2000), *vol.* 422, *pp.* 207–223. Printed in the United Kingdom

An experimental investigation of the relative diffusion of particle pairs in three-dimensional turbulent flow

By SØREN OTT AND JAKOB MANN

Risø National Laboratory, 4000 Roskilde, Denmark

(Received 10 February 2000)

The particle tracking (PT) technique is used to study turbulent diffusion of particle pairs in a three-dimensional turbulent flow generated by two oscillating grids. The experimental data show a range where the Richardson–Obukhov law $\langle r^2 \rangle = C\varepsilon t^3$ is satisfied, and the Richardson–Obukhov constant is found to be $C = 0.5$. A number of models predict much larger values. Furthermore, the distance–neighbour function is studied in detail in order to determine its general shape. The results are compared with the predictions of three models: Richardson (1926), Batchelor (1952) and Kraichnan (1966*a*). These three models predict different behaviours of the distance–neighbour function, and of the three, only Richardson's model is found to be consistent with the measurements. We have corrected a minor error in Kraichnan's (1996*a*) Lagrangian history direct interaction calculations with the result that we had to increase his theoretical value from $C = 2.42$ to $C = 5.5$.

1. Introduction

In a now classical paper Richardson (1926) introduced the concept of relative turbulent diffusion and offered the first theoretical treatment. In order to quantify the growth of a cloud in a turbulent flow Richardson introduced the distance–neighbour function $q(\boldsymbol{r}, t)$, which is defined as the probability density function at time t for the separation $\boldsymbol{r}$ between two fluid particles chosen randomly from a puff released (or marked) at time $t = 0$. The puff can be described by continuous concentration field $c(\boldsymbol{x}, t)$, which we may normalize so that $\int c(\boldsymbol{x}, t)\, \mathrm{d}^3 x = 1$, and we derive the following equation:

$$q(\boldsymbol{r}) = \int \langle c(\boldsymbol{x}) c(\boldsymbol{x} + \boldsymbol{r}) \rangle \, \mathrm{d}^3 \boldsymbol{x}, \tag{1.1}$$

where $\langle\, \rangle$ denotes the ensemble average. When the puff is initially small q does not depend on the detailed initial conditions and thus becomes a universal function (Monin & Yaglom 1975). Assuming homogeneity, isotropy and stationarity, Richardson proposed a simple first-order closure for q

$$\frac{\partial q(r,t)}{\partial t} = \frac{1}{r^2} \frac{\partial}{\partial r} r^2 K \frac{\partial}{\partial r} q(r,t), \tag{1.2}$$

where $K = K(r, t)$ is a diffusivity, and $r = |\boldsymbol{r}|$ is the absolute value of the separation vector $\boldsymbol{r}$. (Actually Richardson used a one-dimensional equation, but that does not change results qualitatively.) Richardson argued further that K is proportional to $r^{4/3}$.

This is consistent with Kolmogorov scaling for the inertial subrange, where K takes the form

$$K = \varepsilon^{1/3} r^{4/3} F(\varepsilon^{1/3} r^{-2/3} t). \tag{1.3}$$

Here ε is the mean rate of dissipation of specific kinetic energy and F is a universal function of the dimensionless argument $s = \varepsilon^{1/3} r^{-2/3} t$. Thus Richardson's model is the case where F is a constant and K is independent of time. Using (1.3) equation (1.2) has the following solution:

$$q(r, t) = \frac{1}{\varepsilon^{3/2} t^{9/2} N} G(\varepsilon^{1/3} r^{-2/3} t), \tag{1.4}$$

where N is a normalization constant and

$$G(s) = \exp\left[\frac{9}{4} \int_1^s \frac{1}{x^2 F(x)} \, \mathrm{d}x\right]. \tag{1.5}$$

Another simple consequence of Kolmogorov scaling is the Richardson–Obukhov law

$$\langle r^2 \rangle = C \varepsilon t^3, \tag{1.6}$$

where C is the Richardson–Obukhov constant. The factor t^3 is due to Richardson, while ε is due to Obukhov (1941), hence the name. Using (1.5) it follows that

$$C = \frac{6\pi}{N} \int_0^\infty s^{-17/2} G(s) \, \mathrm{d}s. \tag{1.7}$$

Batchelor (1952) distinguished three regimes: a regime dominated by the initial velocity difference; the inertial-range regime where (1.6) is valid; and a 'normal' diffusion regime at large separations where the movements of the two particles are uncorrelated. In the following we concentrate on the inertial-range regime.

Of the many attempts to improve and/or substantiate Richardson's theory we limit discussions to two well-known models. The first is due to Batchelor (1952), who argued against K depending on the instantaneous separation variable $\boldsymbol{r}$ and favoured a purely time-dependent diffusivity. This is equivalent to setting $F(s) = s^2$. The second model is Kraichnan's (1996*a*) LHDI (Lagrangian history direct interaction) theory, which yields a diffusion equation for q with a diffusivity of the form (1.3). In LDHI the function $F(s)$ behaves like $F(s) \propto s$ for small s and approaches a constant value for $s \to \infty$. The three models predict quite different behaviours of the distance–neighbour function. In Richardson's model q behaves like $\mathrm{e}^{-|\boldsymbol{r}|^{2/3}}$ with a notable cusp at $\boldsymbol{r} = \boldsymbol{0}$. In contrast, Batchelor's q is smoothly Gaussian. Kraichnan's q looks like Richardson's for small separations ($s \to \infty$), but its tails are different behaving like $\mathrm{e}^{-|\boldsymbol{r}|^{4/3}}$. All three models are consistent with the Richardson–Obukhov law, but C is an adjustable parameter in the models of Richardson and Batchelor. LDHI has no adjustable parameters and hence it predicts C.

Fung *et al.* (1992) pointed out the substantial disagreement between theoretical predictions of the Richardson–Obukhov constant, spanning three orders of magnitude. LDHI (Kraichnan 1966*a*) yields $C = 5.5$ (we have corrected Kraichnan's original value $C = 2.42$, see the Appendix). EDQNM (the eddy-damped quasi-normal Markovian model) yields $C = 3.5$ (Larchevêque & Lesieur 1981). Novikov (1963) estimated $C = 1.8$.

For random flight models, of which there are several, C depends on the choice of model parameters. Reviewing a family of such models Borgas & Sawford (1994) found $0.9 < C < 3.4$ for Thomson's (1990) model and $0.8 < C < 1.8$ for their own

model. Other suggestions are: $C = 6 \times 0.534 = 3.2$ (Mikkelsen, Larsen & Pecseli 1987), $C \approx 0.5$ (Kristensen & Kirkegaard 1987), $C = 1.7$ and 0.17 (Ott 1992), $C = 0.1$ (Fung *et al.* 1992).

Experimental values of C are scarce and based on indirect analyses. Tatarski (1960) found $C = 0.06$, which, according to Fung & Vassilicos (1998), can only be regarded as an order-of-magnitude estimate 'fraught with uncertainties.' Byzova, Garger & Ivanov (1970) used (1.6) and Novikov's value $C = 1.8$ to estimate ε from data for elevated smoke plumes. The resulting values were slightly larger than values of ε derived independently from wind profiles. Turning the argument around, the data are consistent with $C = 1.7$. Several other experiments demonstrate a range where $\langle \boldsymbol{r}^2 \rangle \propto t^3$, but with no measurements of ε (Gifford 1977). Hanna & Briggs (1982) recommends $\sigma_y^2 = 1\,\varepsilon t^3$ for atmospheric puffs. Assuming isotropy this implies $C = 6$ where a factor of three comes from the three spatial components and a factor of two from the conversion from dispersion of two particles relative to the centre of gravity to dispersion relative to each other. It thus appears that not even the second moment of the distance–neighbour function is known with any appreciable degree of accuracy.

Still less is known about the shape of q in three-dimensional flow, and there are diverging opinions. Sullivan (1971), investigating fluorescent dye plumes in Lake Huron, found support for Kraichnan's results. The measurements were taken by means of a flourometer mounted on a boat traversing the plume at high speed. Sullivan correlated the measurements and interpreted the results as a measure of $\iint q(x, y, z, t)\,\mathrm{d}x\mathrm{d}z$, the probability density function for the y-component of the separation vector. This interpretation is questionable given the fact that the dye was released continuously and not as a small and instantaneous puff. The finite spatial resolution of the fluorometer may have also influenced the results and biased the conclusion. Somewhat similar experiments were performed by Jørgensen (1993), who studied passive smoke plumes from ground releases in the atmospheric surface layer. A lidar was used to obtain instantaneous concentration profiles along a horizontal line perpendicular to the plume axis, and the correlation function $p(y, z) = \int \langle c(x, y + y', z)c(x, y', z)\rangle\,\mathrm{d}y'$ (with $z \sim 0$) was analysed and compared with Richardson's and Batchelor's distance–neighbour functions. Jørgensen found p to be definitely peakier around $y = 0$ than Batchelor's Gaussian, solution and consistent with Richardson's, taking into account the finite spatial resolution of the lidar. In a flume experiment Virant & Dracos (1997) found q to be close to Gaussian, in agreement with Batchelor's model. However, the flow was strongly sheared, the puffs studied were larger than the integral length scale of the turbulence, and they were not initially small. Direct numerical simulations of two-particle dispersion were performed by Yeung (1994), who determined q for very long t (43 times the Lagrangian timescale). This is well into the normal diffusion regime where a Gaussian q is expected (and was found).

Recently Jullien, Paret & Tabeling (1999) took measurements in two-dimensional turbulence. PIV (particle image velocimetry) was used to measure the whole velocity field and then this was used to compute fluid particle pair trajectories. The detailed distance–neighbour functions obtained were found to be in good agreement with Richardson's model and inconsistent with Batchelor's model. The present experimental study is similar to this study except that the flow is three-dimensional.

2. The experiment

Three-dimensional particle tracking (PT) is basically a stereometric method yielding trajectories of small particles added to a fluid. A detailed description of the techni-

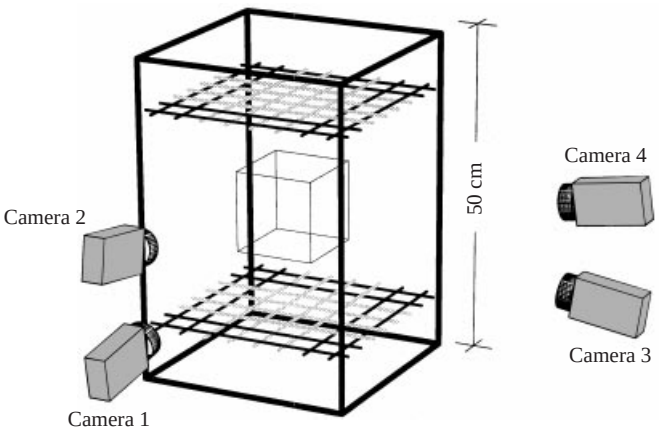

FIGURE 1. The basic system with the tank, the two grids and the four CCD cameras. The box inside the tank is the measuring volume.

calities can be found in Mann, Ott & Andersen (1999). Hence, only brief summary of the experimental design is given here.

2.1. *Apparatus*

A water tank measuring $320 \times 320 \times 450\,\mathrm{mm}^3$ was used for the experiment. The tank was equipped with two grids placed at the top and at the bottom and turbulence was generated by oscillating the grids. The stroke S (peak-to-peak motion) of the grids was set to 50 mm in all runs, while the oscillation frequency F was varied in order to vary the Reynolds number. The average distance between the grids is approximately 300 mm. Two grids are better than one, because a single grid generates a strong secondary flow. The two-grid arrangement has the additional advantage that the spatial variations of turbulence characteristics are small in the region near the plane of symmetry midway between the grids (Dracos 1996).

Video images were taken by four synchronized CCD cameras through two windows in the tank, see figure 1. The four cameras overlook a central volume of the tank measuring roughly $150 \times 150 \times 150\,\mathrm{mm}^3$.

The light source was a Xenon discharge tube yielding 50 μs flashes at a rate of 25 flashes per second synchronous with the cameras. With a discharge energy of 4 J per flash images with good contrast were obtained. The analog output from the cameras was digitized by two computers equipped with commercial frame grabbers and hardware compression cards, and output from the frame grabbers was written continuously to two hard disks. A conventional interlaced technique was used with a camera speed of 50 frames (odd/even line half images) per camera per second. This yields 25 fields (full images) per camera per second. Since both frames of a field are actually exposed by the same flash, it is effectively a 25 Hz non-interlaced technique (Dracos 1996).

The water was seeded with spherical Polystyrene particles with diameters in the range 500–600 μm. A heat treatment was applied to the particles in order to adjust their density to that of the water.

On the raw images particles appear as white dots on a black background. Each dot is two or three pixels wide, which enables the dot centre to be determined with sub-pixel accuracy (Dracos 1996). A dot on an image corresponds to a particle located somewhere on a straight line (ray) inside the tank, and in order to translate dots into lines,

images were taken of an object with known geometry. The object was a transparent box made from 2 mm Perspex sheets with a square mesh of visible marks on each side. The meshes are easily identified on an image and hence each pixel can be associated with a line inside the box. Due to refraction at the tank windows and lens imperfections the translation from pixel positions to lines inside the tank is slightly nonlinear. The calibration box was removed from the tank before the actual experiments.

2.2. *Tracking procedure*

The tracking procedure can be divided into three steps (Malik, Dracos & Papantoniou 1993). The first step is to determine dot positions. The second step is to match dots on the four simultaneous images by identifying intersection points in three dimension. Due to experimental errors, the four lines never intersect exactly at one point and, hence, an *ad hoc* strategy is involved in the selection of best matches. The result of step two is a three-dimensional picture with corresponding three-dimensional particle positions. The third step is to track the particles, i.e. to identify the individual particle trajectories in a sequence of three-dimensional pictures. The tracking is based on a forecasting strategy. More details on the strategies for matching and tracking are described by Mann *et al.* (1999), see also Dracos (1996).

The tracking procedure outlined above is very similar to that of Malik *et al.* (1993). The main difference is that we base the tracking (step three) on the three-dimensional pictures, while Malik *et al.* base it on the separate two-dimensional images and thus perform three-dimensional matching as the last step. We prefer to use the three-dimensional pictures for tracking, because they contain more information than single two-dimensional images.

Several factors affect the accuracy of the determination of particle positions, but roughly they fall into two categories: distortion and jitter. Distortion is caused e.g. by misalignment of the dots on the calibration box and can be characterized as spatially coherent and persistent from picture to picture. Distortion affects absolute spatial positions, and consequently it is less important for the determination of velocities and other quantities based on measurements of short distances. Jitter can be caused by electronic noise in the synchronization signals, mechanical vibrations and errors in the determination of dot centres. Mechanical vibrations can be eliminated by turning off grid oscillations and record tracks of particles that move very slowly. In an almost laminar flow the trajectories are necessarily smooth, and jitter caused by other factors than vibrations can be determined. We find that the r.m.s. value of coordinate jitter is no more than 20 μm, or less than one tenth of the size of a pixel (300 μm). When the grids are operating there will be mechanical vibrations and possibly also electromagnetic interference from the motor. Assuming that the jitter is uncorrelated from picture to picture, the magnitude can be estimated from measured acceleration auto-correlation functions (see Mann *et al.* 1999. This method yields r.m.s. values up to about 60 μm or 0.2 pixels.

3. Results

Below results from six runs are reported. Table 1 gives an overview of some of the basic turbulence parameters and further details may be found in Mann *et al.* (1999).

3.1. *Flow characteristics*

The one-point statistics reveals that $\sigma_u \approx \sigma_v$ and $\sigma_w \approx 1.25\sigma_u$, where w is the velocity component perpendicular to the grids. There is a small secondary flow of the order

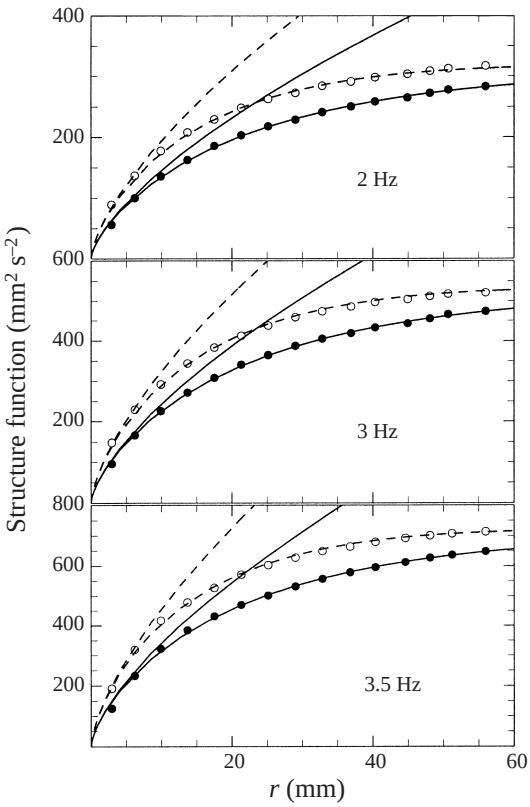

FIGURE 2. Measured longitudinal (dots) and transverse (circles) structure functions from run 17 ($F_{\text{grid}} = 2$ Hz), 15 (3 Hz) and 21 (3.5 Hz). The solid curves are a fit of (3.9) to the data and the corresponding inertial-subrange expression (3.4). The dashed curves are (3.10) and (3.5) using the parameters from the fit.

of $u \approx 0.25\sigma_u$. The secondary flow strengthens if the grids do not have exactly the same distance to the walls.

The longitudinal second-order structure function f is defined as

$$f(r) \equiv \langle \delta v_\parallel^2(r) \rangle, \tag{3.1}$$

where $\delta v_\parallel(r) = \delta \boldsymbol{v}(\boldsymbol{r}) \cdot \boldsymbol{r}/r$ is the radial component of the relative velocity $\delta \boldsymbol{v}(\boldsymbol{r})$ of a pair of particles with separation vector $\boldsymbol{r}$. When $f(r)$ is determined from data an average is taken over all separations $\boldsymbol{r}$ with $|\boldsymbol{r}| = r$ for particle pairs inside the measuring volume. This definition of f makes it an isotropic quantity, even for an anisotropic flow. The transverse structure function g is defined as

$$g(r) \equiv \tfrac{1}{2}(\langle \delta \boldsymbol{v}^2(r) \rangle - \langle \delta v_\parallel^2(r) \rangle). \tag{3.2}$$

Again the average includes averaging over all directions. Due to the isotropy of the *definitions* of f and g it follows solely from incompressibility that (Mann *et al.* 1999)

$$r\langle \delta a_\parallel(r) \rangle = r\, f'(r) + 2f(r) - 2g(r), \tag{3.3}$$

where $\delta a_\parallel(r)$ is the radial component of the relative acceleration. For a globally homogeneous flow the left-hand side of (3.3) vanishes, and we are left with a well-known relation, usually derived as a consequence of isotropy *of the flow*.

Kolmogorov (1941*b*) showed that for inertial-subrange distances

$$f(r) = C_K(\varepsilon r)^{2/3}. \tag{3.4}$$

Using (3.3) with $\langle \delta a_\parallel(r) \rangle = 0$ (3.4) implies

$$g(r) = \tfrac{4}{3} f(r). \tag{3.5}$$

C_K is the Kolmogorov constant. Through a review of many sources Monin & Yaglom (1975) found that $C_K \approx 2.0$. Later Chasnov (1991) found that slightly newer experiments both in the atmosphere and in the laboratory scatter values between 1.75 and 2.75 with an average of $C_K \approx 2.1$. Chasnov also compiled predictions from DNS (and a few LES), having roughly the same Reynolds numbers as the flow in the middle of our tank. These values scatter between 2.1 and 3.2 with a single outlier at 5 and tend to cluster around $C_K \approx 2.6$. A newer collection of high Reynolds number experiments performed both in the atmosphere and in a large wind tunnel in the Reynolds number range $R_\lambda = (2.0\text{–}12.7) \times 10^3$ show a decrease of C_K with Reynolds number, starting at $C_K = 2.5$ at the lower limit and $C_K = 2.1$ at the highest R_λ (Praskovsky & Oncley 1994). It seems that the Monin & Yaglom (1975) value of 2.0 is plausible, but might be somewhat low, at least for lower Reynolds numbers, and that $C_K = 2.5$ could be just as good. The theoretical LDHI value is 2.33 (Kraichnan 1966*b*).

The energy spectrum corresponding to (3.4) and (3.5) is

$$E(k) = \alpha \varepsilon^{2/3} k^{-5/3}, \tag{3.6}$$

where k is the wavenumber, and the relation between C_K and α, the spectral Kolmogorov constant, is (Monin & Yaglom 1975)

$$C_K = \tfrac{27}{55}\Gamma(\tfrac{1}{3})\alpha \approx 1.315\alpha. \tag{3.7}$$

We find that the energy spectrum proposed by von Kármán (1948),

$$E(k) = \alpha \varepsilon^{2/3} L^{5/3} \frac{(Lk)^4}{(1 + (Lk)^2)^{17/6}}, \tag{3.8}$$

where L is a length scale, fits measured data well. It can be shown (assuming isotropy and incompressibility) that the corresponding structure functions are

$$f(r) = \frac{18}{55} \frac{\pi^{1/2} 2^{2/3}}{\Gamma(\frac{5}{6})} \alpha \varepsilon^{2/3} \left\{ \frac{2^{1/3}\pi}{3^{1/2}\Gamma(\frac{2}{3})} - \left(\frac{r}{L}\right)^{1/3} K_{1/3}\left(\frac{r}{L}\right) \right\} \tag{3.9}$$

and

$$g(r) = \frac{18}{55} \frac{\pi^{1/2} 2^{2/3}}{\Gamma(\frac{5}{6})} \alpha \varepsilon^{2/3} \left\{ \frac{2^{1/3}\pi}{3^{1/2}\Gamma(\frac{2}{3})} + \frac{1}{2}\left(\frac{r}{L}\right)^{4/3} K_{2/3}\left(\frac{r}{L}\right) - \left(\frac{r}{L}\right)^{1/3} K_{1/3}\left(\frac{r}{L}\right) \right\}, \tag{3.10}$$

and that these reduce to (3.4) and (3.5) in the limit $r \to 0$. In (3.9) and (3.10) K_n is a modified Bessel function of the second kind.

Examples of measured structure functions are shown in figure 2. We have fitted data for f to (3.9) in order to obtain $\alpha\varepsilon^{2/3}$ and L. These parameters are in turn used to calculate g from (3.10), which is equivalent to using (3.3) with $\langle \delta a_\parallel \rangle = 0$. The dashed curves in the figure therefore represent predictions of g from the measurements of f,

Run	$F_{\rm grid}$ (Hz)	$\alpha\varepsilon^{2/3}$ ($\rm mm^{4/3}\,s^{-2}$)	L (mm)	σ ($\rm mm\,s^{-1}$)	$L_{\rm int}$ (mm)	ε ($\rm mm^2\,s^{-3}$)	τ_η (s)	η (mm)	λ (mm)	R_λ
15	2.96	40	29	16	22	135	0.081	0.27	5.1	93
16	2.97	45	28	17	21	160	0.075	0.26	4.9	91
17	2.00	24	29	12	22	62	0.120	0.33	5.8	81
20	3.50	65	29	21	22	279	0.056	0.22	4.5	104
21	3.45	56	28	19	21	225	0.063	0.24	4.6	97
22	2.00	25	27	12	20	65	0.117	0.32	5.6	78

TABLE 1. Summary of the derived parameters from the second-order structure function.

and clearly they fit the measured values of g very well. Using a plausible value of α (or C_K) this procedure determines ε.

The advantage of this method of obtaining ε is that the second-order structure function can be determined fairly accurately. It is, however, an indirect method which depends on the empirical constant C_K, and alternatives have been considered. Thus it would seem natural to use an exact relation such as Kolmogorov's (1941*a*) four-fifths law

$$\langle \delta v_\parallel^3(r)\rangle = -\tfrac{4}{5}\varepsilon r. \tag{3.11}$$

Unfortunately this is valid only for $R_\lambda \to \infty$ and we are far below that limit. We find the remarkably simple relation

$$\langle \delta \boldsymbol{v}(\boldsymbol{r})\cdot\delta \boldsymbol{a}(\boldsymbol{r})\rangle = -2\varepsilon \tag{3.12}$$

much more useful. A proof based only on local homogeneity and global stationarity is given by Mann *et al.* (1999). These assumptions are weaker than those required to prove (3.11). Note also that an average over directions is not implied in (3.12). Experimental data show that $\langle \delta \boldsymbol{v}(\boldsymbol{r})\cdot\delta \boldsymbol{a}(\boldsymbol{r})\rangle$ is indeed reasonably independent of both the direction and the absolute value of $\boldsymbol{r}$ even when r is well outside the inertial range (Mann *et al.* 1999).

The discrepancy between dissipation rates determined from (3.12) and from the second-order structure function is typically 20%. We take this as an indication of the level of uncertainty in the determined values of ε.

3.1.1. *Derived quantities*

The parameters $\alpha\varepsilon^{2/3}$ and L obtained by the fit to (3.9) are shown in table 1. From these parameters we can calculate the variance of one component of the velocity through the identity

$$\frac{3}{2}\sigma^2 = \int_0^\infty E(k)\,\mathrm{d}k = \frac{27\pi^{1/2}\Gamma(\frac{1}{3})}{110\Gamma(\frac{5}{6})}\alpha\varepsilon^{2/3}L^{2/3}, \tag{3.13}$$

where $E(k)$ is the von Kármán form (3.8). The integral scale is defined via the correlation function $R_\parallel(r) = \sigma^2 - \frac{1}{2}\langle \delta v_\parallel^2(r)\rangle$ as

$$L_{\rm int} \equiv \int_0^\infty R_\parallel(r)\,\mathrm{d}r = \frac{\pi\Gamma(\frac{5}{6})}{\Gamma(\frac{1}{3})}L. \tag{3.14}$$

The energy dissipation ε is finally obtained from $\alpha\varepsilon^{2/3}$ through the relation (3.7) using Monin & Yaglom's 1975 value $C_K = 2.0$.

The Kolmogorov length and time are defined by

$$\eta = \left(\frac{\nu^3}{\varepsilon}\right)^{1/4}, \quad \tau_\eta = \left(\frac{\nu}{\varepsilon}\right)^{1/2}, \tag{3.15}$$

where the kinematic viscosity for water at 27.5 °C is $\nu = 0.89\,\mathrm{mm^2\,s^{-1}}$. According to Hinze (1975) the Taylor microscale λ may be written as

$$\lambda = \left(\frac{15\nu\sigma^2}{\varepsilon}\right)^{1/2} \tag{3.16}$$

and the Taylor microscale Reynolds number as

$$R_\lambda = \frac{\lambda^2}{15^{1/2}\eta^2}. \tag{3.17}$$

All these derived quantities are shown in table 1. It is noted that the governing equations are invariant under a rescaling of the time axis, i.e. the replacement $(F, v, \boldsymbol{u}(\boldsymbol{x}, t)) \mapsto (\beta F, \beta v, \beta \boldsymbol{u}(\boldsymbol{x}, \beta t))$ where β is a number. Since the rescaling preserves boundary conditions it implies an exact similarity of flows having the same value of v/F. The high Reynolds number limit $v \to 0$ can therefore be studied by letting $F \to \infty$. In this limit statistics of the velocity field, scaled so that βF is constant, are expected to converge to finite values. This implies that L, σ/F and ε/F^3 should be independent of F for large F. In the experiment this is reasonably well fulfilled. The standard deviation of L and σ/F are 3% and 4%, respectively, and there is no sign of any systematic variation with F. We take this as an indication that the energy transfer from the grids to the tank centre is independent of the effects of viscosity. Whether the high Reynolds number limit is reached in the central region is more uncertain. The standard deviation of ε/F^3, where ε is measured in the central region, is 17%. The values of ε/F^3 are higher for $F = 2\,\mathrm{Hz}$ than for the two other frequencies, but this variation is within the estimated error bounds of ε.

3.2. *The Richardson–Obukhov law*

Having determined the energy dissipation we now turn to the investigation of Richardson–Obukhov's law for two-particle diffusion

$$\langle |\boldsymbol{r}(\Delta t)|^2 \rangle = C\varepsilon(\Delta t)^3, \tag{3.18}$$

when $\boldsymbol{r}(\Delta t)$ is the vector separating two fluid particles, and $\Delta t = t - t_0$ is time measured from an initial time t_0, when the two particles were close together. The relation is believed to be valid for inertial-subrange separations corresponding to time lags Δt ranging roughly from the Kolmogorov time scale to the Lagrangian integral time scale. Ideally a series of experiments should be made in order to first determine $\langle |\boldsymbol{r}(\Delta t)|^2 \rangle$ in the limit $v \to 0$ (or $F \to \infty$) for a fixed initial separation r_0. Subsequently, the limit $r_0 \to 0$ should be determined. In the actual experiment we have only varied v (i.e. F) by a factor of 2 and r_0 by a factor of 1.5, both without observing any systematic variation of C. In more practical terms the important thing is that r_0 should be inside the inertial range, i.e. $r_0 \gg \eta$ should be obeyed.

In the experiments a large number of particles were added and kept well mixed with the water. No 'puff' of particles was released; instead pairs of particles were selected and their tracks were analysed. This procedure ensures a completely passive and unbiased 'marking' of the pairs.

Examples of tracks of particles that initially are close together are shown in figure 3.

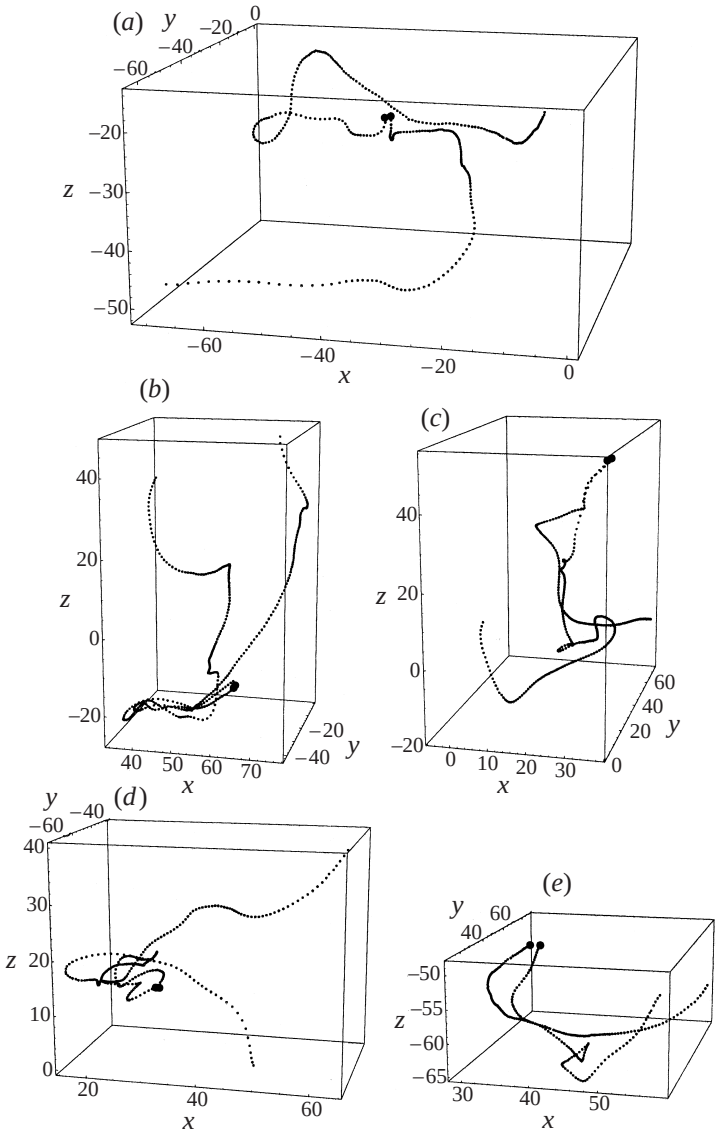

FIGURE 3. Tracks of pairs of particles that are initially within 2 mm of each other. The tracks start with a large black dot. (*a*) and (*b*) from run 20, (*d*) from run 16 and (*c*) and (*e*) from run 17.

Some pairs stay together for a while, others diverge almost immediately. A small initial separation should be preferred, but for smaller initial separations we get fewer pairs, and 3 mm seems to be a good compromise for the present data. Choosing 2 mm does not change the results although it degrades the statistics. With $r_0 \sim 10\eta$ is seems reasonable to assume that the condition $r_0 \gg \eta$ is obeyed.

The resulting averages for all the runs are plotted in figure 4 as $\langle |\boldsymbol{r}(\Delta t)|^2 \rangle^{1/3}$ versus $F\Delta t$. Using the non-dimensional time variable $F\Delta t$ the curves should collapse on a single universal curve if $F \sim \infty$. It appears that they do, at least for the smaller $F\Delta t$. The statistical uncertainty increases with t because the efficiency of the tracking procedure limits the number of long tracks that can be obtained.

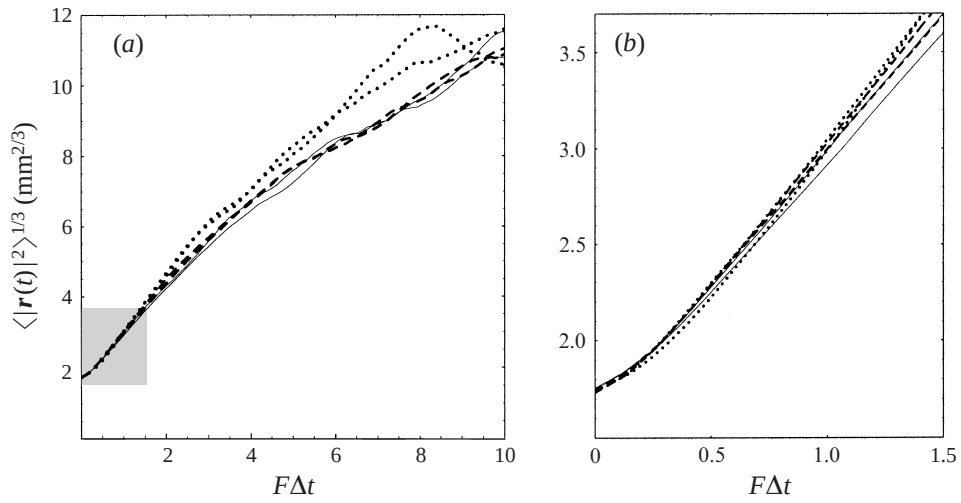

FIGURE 4. (*a*) The mean-squared separation as a function of time. Dotted curves: 2 Hz, continuous curves: 3 Hz, dashed curves: 3.5 Hz. (*b*) Blowup of the gray area in (*a*) representing the inertial range.

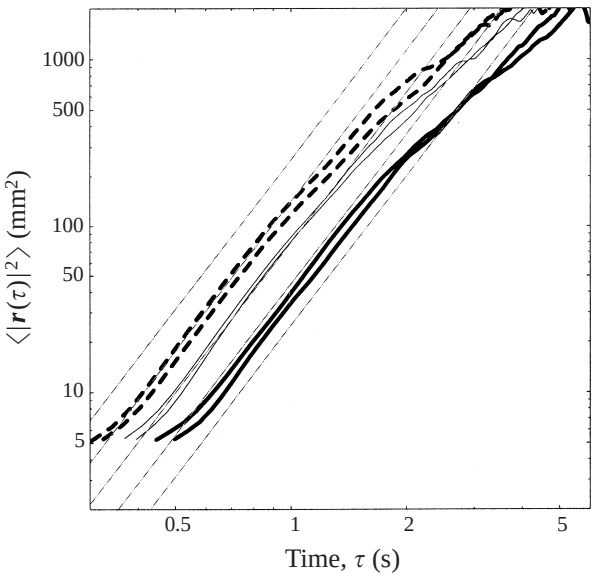

FIGURE 5. A similar plot to figure 4 except that time has been corrected by T_0 and axes are logarithmic. The thin straight lines are $\propto \tau^3$.

The plot should produce straight lines for r in the inertial subrange. Judged from figure 2 the upper end of the inertial range is about 8 mm corresponding to $|\boldsymbol{r}(\Delta t)|^{2/3} \sim 4\,\mathrm{mm}^{2/3}$ or $F\Delta t \sim 1.5$. The linear regime seems to extend somewhat further, up to about $8\,\mathrm{mm}^{2/3}$ where the curves clearly bend away from straight lines. This corresponds to separations equal to L_{int}. For very small $F\Delta t$ the curves deviate from straight lines, but with no sign of any dependence on F. Hence it must be the 'ballistic' regime $\langle \boldsymbol{r}^2 \rangle \sim \langle \boldsymbol{r}_0^2 \rangle + \langle \delta \boldsymbol{v}^2 \rangle \Delta t^2$. The independence of v (F) in this regime confirms that the condition $r_0 \gg \eta$ is fulfilled. Fitting straight lines in the linear,

Run	R_λ	C
15	93	0.56
16	91	0.40
17	81	0.52
20	104	0.49
21	97	0.52
22	78	0.44

TABLE 2. The Richardson–Obukhov constant C for six runs. R_λ (and ε) are determined from the second-order structure function assuming $C_K = 2$.

inertial-range, regime two parameters are obtained: $(C\varepsilon)^{1/3}$ and a zero crossing T_0. There is little variation in the (negative) values of FT_0 for the six curves. The interval $0.5 < F\Delta t < 1.5$ was chosen for these fits. The upper limit corresponds to the inertial range determined from the second-order structure function.

In figure 5 the curves of figure 4 have been translated in time by the amount T_0, i.e. $\tau = \Delta t - T_0$ is used instead of Δt. A τ^3 behaviour is evident.

Table 2 shows measured values of C using ε determined by the second-order velocity structure function method assuming $C_K = 2.0$. The average value is

$$C = 0.5 \pm 0.2. \tag{3.19}$$

The error bounds do not simply indicate the order of magnitude of the experimental scatter, which is ± 0.06. They also include the uncertainties associated with the determination of the energy dissipation ε. Lacking a definite value of C_K is a major source of uncertainty.

3.3. *The distance–neighbour function*

All three models considered here have solutions of the form

$$q(\boldsymbol{r}, t) = \frac{1}{N\langle \boldsymbol{r}^2 \rangle^{3/2}} \exp\left[-H(r/\langle \boldsymbol{r}^2 \rangle^{1/2})\right], \tag{3.20}$$

where N is a normalization constant. For Richardson's model we have

$$N_R = \frac{35}{3}\left(\frac{2\pi}{143}\right)^{3/2}, \quad H_R(\rho) = \left(\frac{1287\rho^2}{8}\right)^{1/3}, \tag{3.21a,b}$$

and for Batchelors's model

$$N_B = \left(\frac{2\pi}{3}\right)^{3/2}, \quad H_B(\rho) = \frac{3\rho^2}{2}. \tag{3.22a,b}$$

Note that N and H are independent of C for both models. For Kraichnan's model, where H does not have an analytic form, we use the numerical results in the Appendix.

In order to estimate $q(r, \tau)$ experimentally, we count the number of pairs in a thin spherical shell of mean radius r at time $\tau = \Delta t - T_0$. By normalizing with the total number of pairs in all the shells at the given τ and dividing by the volume of each shell we get an estimate of $q(r, \tau)$ as a function of r. It is reasonable to restrict the analysis to time lags that are large enough for the distribution to become independent of the initial conditions. Based on figure 4 we believe that this is the case when $0.25 < \Delta t < 1.25$ s. In figure 6 we show a comparison of the three models with the experiment.

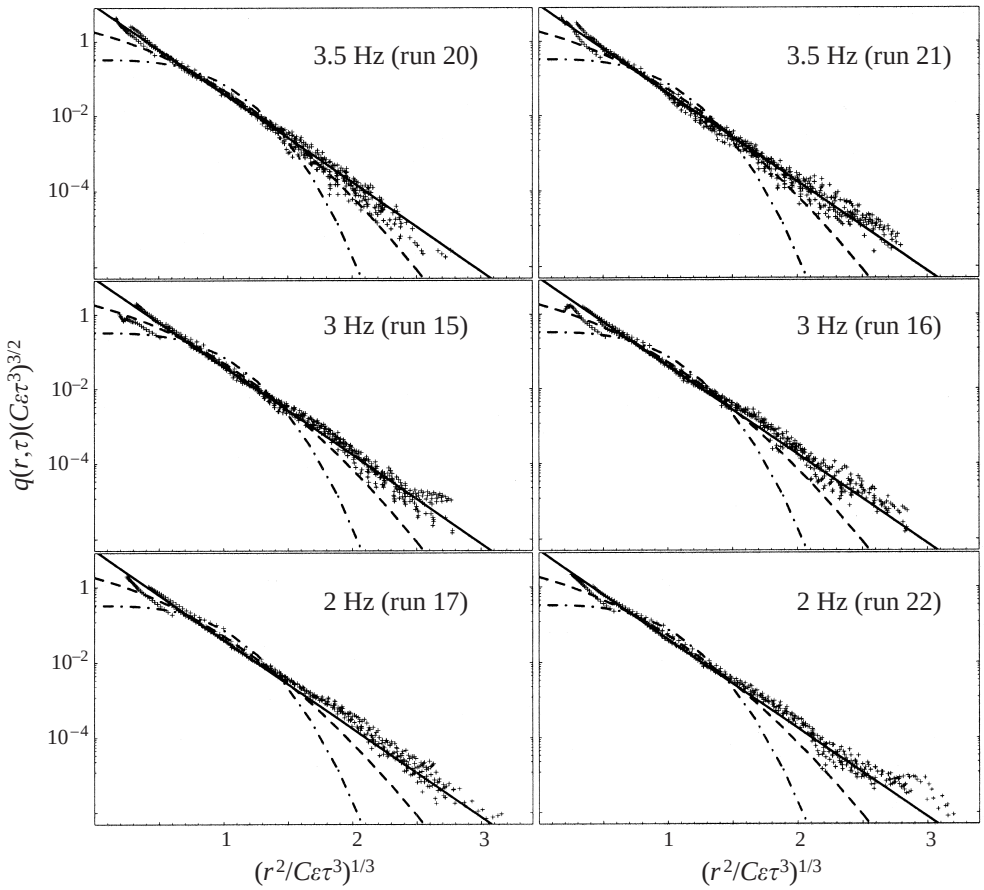

FIGURE 6. Distance–neighbour functions with $0.25 < \Delta t < 1.25$ s compared to the expressions of Richardson ((3.21), solid), Kraichnan (dashed), and Batchelor ((3.22), dot–dashed).

4. Discussion and conclusions

We find that particle tracking is a promising technique which yields accurate Lagrangian data. The three-dimensional two-grid turbulence ($R_\lambda \approx 100$) is roughly isotropic with a small secondary flow and the second-order structure functions are consistent with a von Kármán spectrum. The inertial range, as judged from the second-order structure function, is quite limited extending up to separations of about 8 mm or one third the integral length scale.

We find that the Richardson–Obukhov law is obeyed in the inertial range. The estimated value of the Richardson–Obukhov constant is $C = 0.5 \pm 0.2$. The law remains valid up to separations comparable to the integral length scale, so that the inertial range appears to be larger for two-particle diffusion than judged from the second-order structure function. For the third-order structure function there is, on the other hand, no inertial-range at all (Mann *et al.* 1999). However, such definitions, which merely indicate where this or that quantity exhibits the expected inertial-range behaviour, do not ensure that the infinite Reynolds number limit is actually met. We did not detect any obvious Reynolds number dependence, but the range of Reynolds

numbers obtained was also quite narrow. The experimental results therefore do not rule out the possibility that C depends weakly on the Reynolds number.

Experimental results for the distance–neighbour function are shown in figure 6. Data points collapse on a single curve, as expected for the inertial range.

The agreement between the data and Richardson's expression (3.21) for the distance–neighbour function is excellent. It is also clear that the results are incompatible with Batchelor's model. Kraichnan's model falls somewhere in between, but clearly it does not fit the data. The data show no evidence of the change of behaviour between small and large values of $(r^2/C\varepsilon\tau^3)^{1/3}$ that characterizes Kraichnan's model. The predictions presented here for Kraichnan's model are based on a Kolmogorov spectrum, i.e. an infinitely wide inertial range, and it could be argued that a von Kármán spectrum is more appropriate. However, it is not likely that the finite length scale in the von Kármán spectrum is important, because it is larger than the separations of the particle pairs in question. If anything, we expect that such a calculation would merely push Kraichnan's solution towards Batchelor's and thus increase the difference between data and the model. The simplest generalization of these experimental results is to expect Richardson's solution also to be valid at higher Reynolds numbers.

The corrections made in the Appendix change the value of C obtained from Kraichnan's model from 2.42 to 5.5.

There appears to be a conflict between our results and the recent measurements by Virant & Dracos (1997), made at comparable R_λ, who find an excellent agreement with Batchelor's expression (3.22). However, their initial puff is larger than the integral scale, so the experiment is not relevant for relative diffusion within inertial-subrange distances. At the same time it should be noted that Jullien *et al.* (1999) arrive at conclusions similar to ours for two-dimensional turbulence. Their value of C is 0.5, incidentally the same as we find for three-dimensional turbulence.

The value $C = 1.7$ found in atmospheric experiments by Byzova *et al.* (1970) seems to disagree with our result. A Reynolds number dependence is not the only possible explanation. Shear or the presence of a non-zero heat flux could be important. It should also be realized that the experiment addresses the related, yet different problem of dispersion of a plume from an elevated continuous source. The plume width is assumed to be equal to the width of a corresponding puff, which may not be correct. The plume can of course be regarded as a series of puffs, like pearls on a string, where the string represents the line through the puff centres. If this line is relatively straight and the puffs are more or less round balls, it is clear that the plume width is equal to the puff width. On the other hand, if the line is meandering or even occasionally forming an S-shape, which plumes are known to do, then the plume width clearly must be larger than the puff width.

It is thought-provoking that Richardson's model, the oldest of them all, seems to be most realistic. The scope of Richardson's model does not go much beyond solving this particular problem, and the same can be said of Batchelor's model. Contrary to this, Kraichnan's LDHI approximation is a grand scheme designed as a general attack on turbulence problems. As such it has been the subject of much admiration (Leslie 1973), and, although now old, it is still regarded as one of the most serious attempts. It is therefore discouraging that the predicted value of C is ten times too large, especially since LHDI has been applied successfully to a number of other turbulence problems (Leslie 1973). The fact that the measured value $C = 0.5$ is smaller than most models predict indicates a serious lack of understanding of the relative diffusion problem.

	C	$CC_K^{-3/2}$	$\langle \boldsymbol{r}^4\rangle/\langle \boldsymbol{r}^2\rangle^2$	$\langle \boldsymbol{r}^6\rangle/\langle \boldsymbol{r}^2\rangle^3$
Kraichnan (1966*a*)	2.42	0.68	2.27	8.86
Fitted	2.42	0.68	2.26	8.74
Corrected	5.5	1.6	2.3	9.7

TABLE 3. Original and corrected values for LHDI predictions.

The two-particle problem is simple, yet non-trivial and therefore an ideal test case for turbulence modelling. For a long time technical difficulties connected with Lagrangian measurements have prevented this interplay between theory and experiments. A cure for this situation is the development of experimental techniques of which particle tracking seems to be particularly promising.

We thank Professor Arkady Tsinober of Tel Aviv University, Dr Bjarne Stenum and Mr Jan Nielsen, both of Risø, for many important suggestions for the design of the experiment. Most welcome criticisms from Dr Leif Kristensen, Professor Hans Pecseli, Dr Torben Mikkelsen and many others have improved the work substantially. Financial support from the Danish Technical Research Council (STVF) under contract 9601244 is gratefully acknowledged.

Appendix. A correction to Kraichnan's derivation of C

Kraichnan (1966*a*) uses the following solution to (1.2):

$$q'(r,t) = \frac{1}{N'(\varepsilon t^3)^{3/2}} \exp\left(-\frac{9}{4sF(s)}\right), \tag{A 1}$$

where N' is a normalization factor and $s = \varepsilon^{1/3} r^{-2/3} t$. This solution, Kraichnan writes, was suggested by the solutions of Richardson (1926) and Roberts (1961) for the case where F is independent of t. However, comparing (A 1) and (1.5) it is clear that q' is only a solution to (1.2) if F is a constant. In this Appendix we estimate C using the correct solution (1.5). Solving the full set of LHDI equations is, however, rather tedious, so we make the following shortcut. In LHDI F (called $J_\parallel$ in Kraichnan's notation) is equal to

$$F(s) = 4\alpha \int_0^s \mathrm{d}s' \int_0^\infty \mathrm{d}\lambda \left(\frac{1}{3} - \frac{\sin\lambda}{\lambda^3} + \frac{\cos\lambda}{\lambda^2}\right) \frac{R(s'\lambda^{2/3})}{\lambda^{5/3}}, \tag{A 2}$$

where R is a correlation function for Kraichnan's generalized velocity field. R can be determined by numerical solution of the turbulence part of the LHDI equations (Kraichnan 1966*b*, *c*), but we make a shortcut and use the fitted analytic expression

$$R(\xi) = \frac{1}{1 + (\frac{1}{2}\pi\xi/I_R)^2}, \tag{A 3}$$

where $I_R = \int_0^\infty R(\xi)\,\mathrm{d}\xi \approx 1.87$ (Kraichnan 1966*b*). The numerical solution to (A 2) turns out to be represented well by the simple expression

$$F(s) \approx \frac{as}{1+bs}, \tag{A 4}$$

where the constants a and b are determined so as to yield the correct limit of $F(s)/s$

for $s \to 0$ and the correct value of $F(s)$ for $s = 2$. Table 3 shows values of C, $CC_K^{-3/2}$, $\langle \boldsymbol{r}^4 \rangle / \langle \boldsymbol{r}^2 \rangle^2$ and $\langle \boldsymbol{r}^6 \rangle / \langle \boldsymbol{r}^2 \rangle^3$. The first row contains Kraichnan's values. The values in the second row are similar to Kraichnan's except that the analytic fit to F was used. The third row contains corrected values based on the solution (1.5) and the fitted F. The recalculated values in the second row indicate a fairly good fit with numerical errors limited to a few percent. The new value $C = 5.5$ is more than twice as big the old one.

Kraichnan uses $\alpha = 1.77$, which is the value determined by LHDI. This corresponds to $C_K = 2.33$, which is slightly different from the value $C_K = 2$ used to determine ε from the data. We have listed $CC_K^{-3/2}$ because its experimental value is independent of C_K.

REFERENCES

Batchelor, G. K. 1952 Diffusion in a field of homogeneous turbulence. II The relative motion of particles. *Proc. Camb. Phil. Soc.* **48**, 345–363.

Borgas, M. S. & Sawford, B. L. 1994 A family of stochastic models for two-particle dispersion in isotropic homogeneous stationary turbulence. *J. Fluid Mech.* **279**, 69–99.

Byzova, N. L., Garger, Y. K. & Ivanov, V. N. 1970 Experimental estimation of the Lagrangian time scale of turbulence. *Izv. Atmos. Ocean. Phys.* **6**, 315–320.

Chasnov, J. R. 1991 Simulation of the Kolmogorov inertial subrange using an improved subgrid model. *Phys. Fluids* A **3**, 188–200.

Dracos, T. 1996 Three-dimensional velocity and vorticity measuring and image analysis techniques. *ERCOFTAC Lecture Notes*, Vol. 4. Kluwer.

Fung, J. C. H., Hunt, J. C. R., Malik, N. A. & Perkins, R. 1992 Kinematic simulation of homogeneous turbulence by unsteady random Fourier modes. *J. Fluid Mech.* **236**, 281–318.

Fung, J. C. H. & Vassilicos, J. C. 1998 Two-particle dispersion in turbulent like flows. *Phys. Rev.* E **57**, 1677–1690.

Gifford, F. A. 1977 Tropospheric relative diffusion observations. *J. Appl. Met.* **16**, 312.

Hanna, S. R. & Briggs, G. A. 1982 Handbook of atmospheric diffusion. *Tech. Rep.* DE82002045 (DOE/TIC–11223), US Dept. of Energy, US Department of Commerce, Springfield, VA 22161.

Hinze, J. O. 1975 *Turbulence*, 2nd edn. McGraw-Hill.

Jørgensen, H. E. 1993 Studies of concentration fluctuations in the atmospheric surface layer. PhD thesis, Risø National Laboratory.

Jullien, M.-C., Paret, J. & Tabeling, P. 1999 Richardson pair dispersion in two-dimensional turbulence. *Phys. Rev. Lett.* **82**, 2872–2875.

Kármán, T. von 1948 Progress in the statistical theory of turbulence. *Proc. Nat. Akad. Sci.* **34**, 530–539.

Kolmogorov, A. N. 1941*a* Dissipation of energy in the locally isotropic turbulence. *Dokl. Akad. Nauk SSSR* **32**(1). English translation in *Proc. R. Soc. Lond.* A (1991) **434**, 15–17.

Kolmogorov, A. N. 1941*b* The local structure of turbulence in incompressible viscous fluid for very large Reynolds numbers. *Dokl. Akad. Nauk SSSR* **30**(4). English translation in *Proc. R. Soc. Lond.* A (1991) **434**, 9–13.

Kraichnan, R. H. 1966*a* Dispersion of particle pairs in homogeneous turbulence. *Phys. Fluids* **10**, 1937–1943.

Kraichnan, R. H. 1966*b* Isotropic turbulence and inertial-range structure. *Phys. Fluids* **9**, 1728–1752.

Kraichnan, R. H. 1966*c* Lagrangian-history closure approximation for turbulence. *Phys. Fluids* **8**, 575–598.

Kristensen, L. & Kirkegaard, P. 1987 Puff kinematics. *Tech. Rep.* R–548. Risø National Laboratory.

Larchevêque, M. & Lesieur, M. 1981 The application of eddy-damped Markovian closures to the problem of dispersion of particle pairs. *J. Méc.* **20**, 113–134.

Leslie, D. C. 1973 *Developments in The Theory of Turbulence*. Clarendon.

Malik, N. A., Dracos, T. & Papantoniou, D. A. 1993 Particle tracking velocimetry in three-dimensional flows. Part ii: Particle tracking. *Exps. Fluids* **15**, 279–294.

MANN, J., OTT, S. & ANDERSEN, J. S. 1999 Experimental study of relative, turbulent diffusion. *Tech. Rep.* Risø–R–1036(EN). Risø National Laboratory.

MIKKELSEN, T., LARSEN, S. E. & PECSELI, H. L. 1987 Diffusion of Gaussian puffs. *Q. J. R. Met. Soc.* **113**, 81–105.

MONIN, A. S. & YAGLOM, A. M. 1975 *Statistical Fluid Mechanics*, Vol. 2. The MIT Press.

NOVIKOV, Y. A. 1963 Random force method in turbulence theory. *Sov. Phys. JETP* **17**, 1449–1453.

OBUKHOV, A. M. 1941 Spectral energy distribution in turbulent flow. *Izv. Akad. Nauk SSSR* **5**, 453–566.

OTT, S. 1992 Perturbative methods in turbulence and turbulent diffusion. PhD thesis, University of Copenhagen.

PRASKOVSKY, A. & ONCLEY, S. 1994 Measurements of the Kolmogorov constant and intermittency exponent at very high Reynolds number. *Phys. Fluids* **6**, 2886–2888.

RICHARDSON, L. F. 1926 Atmospheric diffusion shown on a distance-neighbour graph. *Proc. R. Soc. Lond.* A **110**, 709–737.

ROBERTS, P. H. 1961 Analytical theory of turbulent diffusion. *J. Fluid Mech.* **11**, 257.

SULLIVAN, P. J. 1971 Some data on the distance-neighbour function for relative diffusion. *J. Fluid Mech.* **47**, 601–607.

TATARSKI, V. I. 1960 Radiophysical methods of investigating atmospheric turbulence. *Izv. Vyssh. Uchebn. Zaved. Radiofiz.* **5**, 551.

THOMSON, D. J. 1990 A stochastic model for the motion of particles pairs in isotropic high-Reynolds-number turbulence, and its application to the problem of concentration variance. *J. Fluid Mech.* **210**, 113–153.

VIRANT, M. & DRACOS, T. 1997 3D PTV and its application on Lagrangian motion. *Meas. Sci. Technol.* **8**, 1529–1552.

YEUNG, P. K. 1994 Direct numerical simulation of two-particle relative diffusion in isotropic turbulence. *Phys. Fluids* **6**, 3416–3428.